Nanoscale

PAPER

View Article Online
View Journal | View Issue

Cite this: *Nanoscale*, 2023, **15**, 8270

Fluorescence labeling methods influence the aggregation process of α-syn *in vitro* differently†

S. Jadavi,[a,b] S. Dante,[c] L. Civiero,[d,e,f] M. Sandre,[f,g] L. Bubacco,[d,e,f] L. Tosatto,[‡h] P. Bianchini,[a] C. Canale[*b] and A. Diaspro[a,b]

In a previous study, the coexistence of different aggregation pathways of insulin and β-amyloid (Aβ) peptides was demonstrated by correlative stimulated emission depletion (STED) microscopy and atomic force microscopy (AFM). This had been explained by suboptimal proteins labeling strategies that generate heterogeneous populations of aggregating species. However, because of the limited number of proteins considered, the failure of the fluorescent labeling that occurs in a large portion of the aggregating fibrils observed for insulin and Aβ peptides, could not be considered a general phenomenon valid for all molecular systems. Here, we investigated the aggregation process of α-synuclein (α-syn), an amyloidogenic peptide involved in Parkinson's disease, which is significantly larger (MW ~14 kDa) than insulin and Aβ, previously investigated. The results showed that an unspecific labeling procedure, such as that previously adopted for shorter proteins, reproduced the coexistence of labeled/unlabeled fibers. Therefore, a site-specific labeling method was developed to target a domain of the peptide scarcely involved in the aggregation process. Correlative STED–AFM illustrated that all fibrillar aggregates derived from the aggregation of α-syn at the dye-to-protein ratio of 1 : 22 were fluorescent. These results, demonstrated here for the specific case of α-syn, highlight that the labeling artifacts can be avoided by careful designing the labeling strategy for the molecular system under investigation. The use of a label-free correlative microscopy technique would play a crucial role in the control of the setting of these conditions.

Received 3rd October 2022,
Accepted 12th April 2023

DOI: 10.1039/d2nr05487f

rsc.li/nanoscale

Introduction

Over the past decade correlative techniques have emerged to integrate information derived from two or more alternative sources. Compared with a single technique, correlative techniques allow the integration of different approaches to achieve better accuracy in the prediction/characterization of biomolecular processes.[1]

In particular, correlative microscopy is based on the coupling of techniques that can provide local multifunctional characterization of the sample.[2,3] The most widespread correlative microscopy applications are related to the coupling of electron and optical microscopy.[4–7] However, in recent years, the integration between atomic force microscopy (AFM) and super-resolution (SR) fluorescence microscopy has been proposed as a primary method in the study of bio-systems.[3,8–12] The substantial advantage of this approach is the inherent capability of both techniques to work in a liquid environment, enabling simultaneous investigation of living systems, such as cells, or dynamic molecular processes, in a physiological-like environment, and at molecular-scale resolution.

Initially, the main idea of coupling AFM with SR[8–11] was to endow AFM with chemical specificity, overcoming one of the most significant limitations of this tool. More recently, new results demonstrated that AFM can assume a key role in testing and validating results obtained by fluorescence microscopy.[12]

It is known that the presence of fluorescent dye molecules can influence molecular processes, although the final effect induced by fluorophores on the molecular mechanisms is difficult to predict. In recent work by our group, the aggrega-

[a]*Nanoscopy, CHT Erzelli, Istituto Italiano di Tecnologia, Via Enrico Melen 83, Building B, 16152 Genova, Italy*
[b]*Department of Physics, University of Genova, Via Dodecaneso 33, 16146 Genova, Italy. E-mail: claudio.canale@unige.it*
[c]*Materials Characterization Facility, Istituto Italiano di Tecnologia, Via Morego 30, 16163 Genova, Italy*
[d]*Department of Biology, University of Padova, Via U. Bassi 58/b, 35131 Padova, Italy*
[e]*IRCCS San Camillo Hospital, Via Alberoni 70, 30126 Venice, Italy*
[f]*Centro Studi per la Neurodegenerazione (CESNE), University of Padova, 35131 Padova, Italy*
[g]*Parkinson and Movement Disorders Unit, Department of Neuroscience, University of Padova, Via Nicolò Giustiniani, 5, 35128 Padova, Italy*
[h]*Istituti di Biofisica, CNR, Trento, Italy*

†Electronic supplementary information (ESI) available. See DOI: https://doi.org/10.1039/d2nr05487f

‡Current address: Centre for Structural Biology, Fondazione Human Technopole, Milan, Italy.

tion process of misfolded peptides was studied. It was already known that the presence of a fraction of fluorescently labeled monomers significantly slowed the aggregation rates of peptides *in vitro*, with an effect proportional to the ratio of labeled molecules.[13,14] Correlative AFM and stimulated emission depletion (STED) fluorescence microscopy demonstrated that unexpected phenomena could affect the aggregation of a partially labeled peptide solution.[12] Specifically, by studying the aggregation of partially labeled solution of insulin or Aβ, it was found that only a fraction of the final fibrillary aggregates was fluorescent. These results indicated that the labeled monomers are involved only in preferred aggregation pathways, while others are precluded. The peculiar asymmetric distribution of the fluorophore in a sample, derived from a process that was in principle considered stochastic, was observed for the first time because of the new capability offered by correlative microscopy. This finding focuses the attention on an issue that involved all fluorescence-based experimental techniques, namely, the validity of results obtained when the molecules have preferential interactions depending on the presence of the fluorescent tag.

We thought that this issue has primary importance for all the investigations based on fluorescence, but we also knew that the unexpected scenario highlighted in our work, obtained for insulin and Aβ peptides, cannot be automatically extended to all the molecular systems that must be studied for their peculiarity.

Both Aβ and insulin are small peptides (MW 4–6 kDa), and the addition of the dye molecule (MW 0.98 kDa) strongly changes the mass of the peptides. In the case of insulin, we covalently bind the fluorophore to amine groups, *i.e.*, more than one fluorophore can bind to a single peptide.

To take this step further, we studied a similar process, *i.e.*, the formation of amyloid fibrils *in vitro*, using a different peptide and a well-controlled labeling method, widely employed in previous works.[15,16] The protein was α-synuclein (α-syn), which is involved in the neurodegenerative cascade in Parkinson's disease. α-syn is larger (MW ~14 kDa) than insulin and Aβ, previously investigated. The fluorophore was covalently bound to the C-terminal group of the peptide, an area of the polypeptide chain not or poorly involved in fibrillation, as suggested in previous works.[15,17,18] We found that all the fibrillar aggregates obtained with a dye-to-protein ratio of 1 : 20 were fluorescent. As a control, we labeled α-syn with NHS-dye, binding the fluorophore at the free amine groups, and using the same dye-to-protein ratio we found that just a subpopulation of fibrils were fluorescent, confirming of the results obtained by Cosentino *et al.*[12]

The molecular size of the protein does not guarantee to avoid influence on the aggregation upon binding of a fluorophore, suggesting the adoption and development of specific fluorophore conjugation strategies. AFM–STED correlative microscopy allows the characterization of the sample at the single fibril level, emerging as a primary tool in the control of the fluorescence distribution in supramolecular samples.

Experimental

Site-specific labeling of α-syn and fibrillation

To produce ATTO 488-labeled fibrils specifically labeled at the α-syn C-terminal end, an α-syn monomer, with Gly-Cys residues at C-terminal (α-synGC) was prepared as described previously[19] and labeled with thiol-reactive ATTO 488-label (ATTO 488-maleimide, ATTO-TEC GmbH) following a "solid state-based labeling" technique.[20] Briefly, expressed, and purified α-synGC cysteine dimers were reduced with 5.23 mM TCEP (tris(2-carboxyethyl) phosphine (Sigma-Aldrich) in NaP buffer 100 mM at pH 7 for 6 hours at room temperature (RT). The resulting monomer-containing solution was diluted 1 : 1 in ultrapure water (Milli-Q, resistivity 18 MΩ cm) and EDTA (1 mM) pH 8, followed by the addition of 70% ammonium sulfate salt (w/v). The labeling reaction was achieved by adding 7 molar equivalents of ATTO 488-maleimide dye (in DMF) and incubating at RT, with no agitation. Labeled α-synGC was precipitated by centrifugation (20 000*g*, 10 min, 4 °C) and the pellet was washed five times with 70% ammonium sulfate in NaP buffer 50 mM pH 7.0. Finally, the pellet was resuspended in PBS and the exceeding dye was removed through PD-10 column (GE Healthcare). ATTO 488 labeled α-synGC was confirmed by RP-HPLC (protein labeling more than 90%) (Fig. S1†). ATTO 488-labeled α-syn fibrils were obtained from LPS-free recombinant human α-syn monomers and ATTO 488 labeled α-syn, incubated in 1 : 22 ratio at a final concentration of 5 mg ml^{-1} in sterile PBS (Biowest). Fibrils were recovered by centrifugation after shaking the sample (ThermoMixer F1.5 Eppendorf, 1000 rpm) at 37 °C for seven days.

Labeling α-syn with NHS-reactive ATTO 488-label and fibrillation

To obtain randomly labeled ATTO 488 α-syn fibrils, an α-syn WT monomer was prepared as described previously[19] and labeled with NHS-reactive ATTO 488-label (ATTO 488-NHS, ATTO-TEC GmbH) following manufacture instructions. Briefly, expressed and purified α-syn WT proteins were labeled with 1.5 molar equivalents of ATTO 488-NHS (ATTO 488-NHS) dye (in DMSO) and incubated at RT 2 hours, with no agitation. To remove the exceeding dye, the reaction was loaded in a PD-10 column (GE Healthcare) and only the conjugated protein was collected.

We provide a detailed quality control for the NHS reaction (see ESI Fig. 1†). As expected, the NHS reaction generates a heterogeneous population of Atto-synuclein species making very difficult the calculation of the number of dye molecules per protein (ESI Fig. 1B–F†). On the other hand, we were able to deduce an approximate value of the overall labeling efficiency that is close to 90%, similarly to the labeling with ATTO 488-maleimide. We can consider that also in this case the approximative labeled to unlabeled monomer ratio is 1 : 22; in any case, the main message of this work does not change for a small deviation of this ratio.

ATTO 488-labeled α-syn (NHS) fibrils were obtained from LPS-free recombinant human α-syn monomers and ATTO 488

labeled α-syn (NHS), incubated in a 1 : 22 ratio at a final concentration of 5 mg ml^{-1} in sterile PBS (Biowest). Fibrils were recovered by centrifugation after shaking the sample (ThermoMixer F1.5 Eppendorf, 1000 rpm) at 37 °C for seven days.

Electron microscopy analysis

Characterization of α-syn fibrils was performed by transmission electron microscopy (TEM) using negative staining. Fibrils samples (1 mg ml^{-1}) were diluted 1 : 22 in ultrapure water (Milli-Q, resistivity 18 MΩ cm) and a 5 μl drop deposited on a copper grid (Sigma-Aldrich), washed twice, and directly stained with 2% uranyl acetate. Fibril samples were examined by TEM (FEI Tecnaii G2) operated at 80 kV with an OSIS Veleta CCD 4-megapixel camera (Olympus).

Correlative AFM–STED

Small aliquots of α-syn fibrils solution were diluted 50-fold in ultrapure water (Milli-Q, resistivity 18 MΩ cm). 100 μl of diluted fibrils were deposited on an oxygen plasma-treated glass coverslip, using a Tucano (Gambetti Kenologia, Italy) setup. The coverslip was treated by applying three 180 s cycles with a power of 100 W, and an oxygen flow of 13 SCCM. Fibrils were let to adhere to the glass substrate for 20 min before gently rinsing with Milli-Q water to remove the fraction of unbound fibrils, and salts present in the aggregation medium. The samples were dried under a gentle nitrogen flow.

A NanoWizard II AFM head (JPK, JPK Instruments, Berlin, Germany) was mounted on a commercial Leica TCS SP5 gated STED-CW microscope. The optical microscope stage was exchanged with an AFM compatible stage (JPK Instruments, Berlin, Germany), which features minimum mechanical coupling of noise to the AFM cantilever.

The STED images have been collected by a hybrid detector in the spectral range of 500–570 nm. We used an HCX PL APO CS 100× 1.4NA oil objective (Leica Microsystems, Mannheim, Germany) and a scan speed of 1400 Hz for 1024 pixels per line with a 128-line average and a time-gated detection of 1.4 ns. The selected dye was ATTO 488 for α-syn, which is suitable for 488 nm excitation and 592 nm depletion wavelengths.

AFM images have been acquired in the air in intermittent contact mode, using a rectangular silicon cantilever (TESPA, Bruker, MA, USA) with a nominal spring constant of 42 N m^{-1}, resonance frequency of 320 kHz, and a tip with a curvature radius of 8 nm. All images were acquired as 512 × 512 pixels images with a scan rate between 0.6 and 1.0 Hz. The Direct Overlay software (JPK Instruments, Berlin, Germany) was used to assist the choice of the overlapped areas in AFM and STED images.[12]

The level of co-localization between AFM and optical images was calculated by using the co-localization function of ImageJ (Bethesda, USA) and deriving the ratio of co-localization. The ratio of co-localization is provided by the Mander's coefficient (see eqn (1)) that provides a quantification of the number of the intensities of the STED image pixels (STED$_i$) that have a correspondence in the AFM image pixel (AFM$_i$) divided by the total sum of AFM image intensity.

$$M_{\mathrm{AFM}} = \frac{\sum_i \mathrm{AFM}_{i,\mathrm{coloc}}}{\mathrm{AFM}_i} \quad (1)$$

$\mathrm{AFM}_{i,\mathrm{coloc}} = \mathrm{STED}_i$ if $\mathrm{AFM}_i > 0$. $M = 1$ is the perfect colocalization, $M = 0$ represent the lack of correlation. The threshold was automatically determined by the software using the Costes auto threshold method.[21] The scatter plots of the pixel-by-pixel correlation were also calculated using the same ImageJ function (Fig. S2†).

Results and discussion

Alpha-syn fibrillation

After 7 days of incubation in the conditions described above, fibrillary aggregates were formed. Fig. 1 shows negative stained TEM images of WT α-syn fibrils unlabeled (a and b), Cys

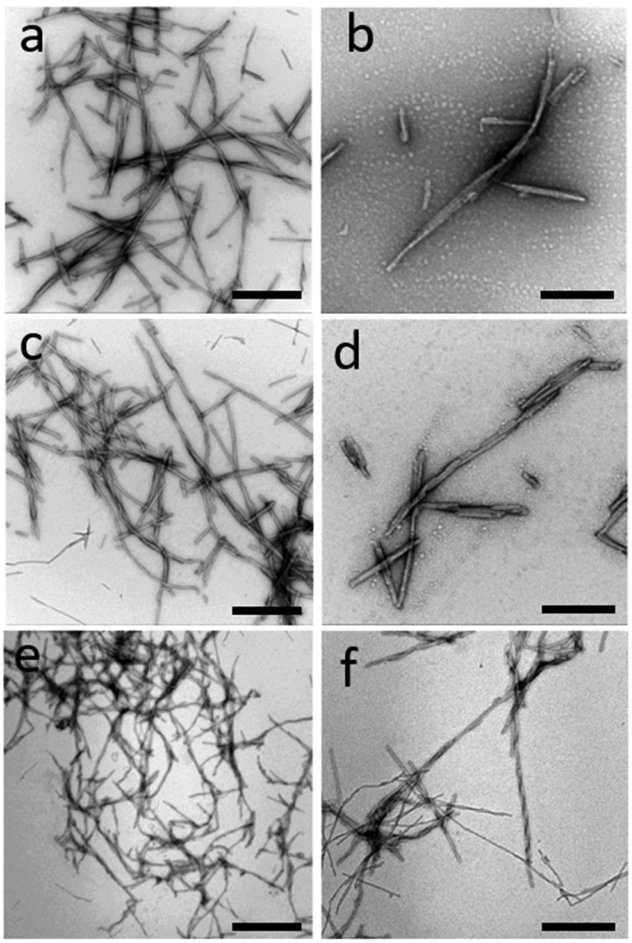

Fig. 1 Negative stained TEM images of WT α-syn fibrils unlabeled (a and b), Cys-mutant α-syn fibrils labeled with ATTO488-maleimide at dye-to-protein ratio of 1 : 22 (c and d), and WT α-syn fibrils labeled with ATTO 488-NHS at dye-to-protein ratio of 1 : 22 (e and f). Scale bar: 1 μm (a, c and e) and 500 nm (b, d and f).

mutant α-syn labeled with ATTO 488-maleimide at dye-to-protein ratio of 1 : 22 (c and d), and WT α-syn fibrils labeled with ATTO 488-NHS at dye-to-protein ratio of 1 : 22 (e and f) (see Experimental section). Fibrils morphology was not strongly affected by the presence of dye molecules. We found a large population of short fibrils that we characterized with both AFM, STED, and TEM. Fibrils length is generally less than 1 μm. Fibrils thickness, calculated from AFM images (see representative images in Fig. S3†), is relatively heterogeneous and is not affected by the presence of the ATTO488-maleimide dye. On the contrary, fibrils thickness is influenced by the presence of ATTO 488-NHS dye. In particular, the average aggregates thickness is 9.7 ± 2.3 nm (mean ± SD) for unlabeled fibrils, 9.6 ± 3.5 nm for ATTO488-maleimide labeled fibrils, and 6.7 ± 1.7 nm for ATTO 488-NHS labeled fibrils. The populations of unlabeled and ATTO488-maleimide label fibrils are comparable, while ATTO 488-NHS label fibrils are significantly thinner ($P > 0.05$). Representative AFM images of the different kind of fibrils are shown in Fig. S3.†

Correlative AFM–STED microscopy

The characterization of the aggregation process of amyloidogenic peptides by advanced correlative techniques is a new way to shed light on understanding the influence that fluorophores have on intermolecular processes. Indirectly, the technique can provide information on the high heterogeneity and multi-pathways behavior of fibrillation. In particular, the mutual and complementary capabilities of correlative AFM–STED nanoscopy enable the observation of selective interaction phenomena, happening during the formation of fibrillar aggregates. A previous study, performed by Cosentino *et al.*[12] on insulin and Aβ peptides suggested that the presence of fluorophores not only decreased the rate of the aggregation, a very well-known effect, but also promoted the coexistence of different aggregation pathways, and that labeled molecules can follow selectively just some of these pathways. In the Cosentino's paradigm, only relatively short peptides were considered, and, in particular for insulin, the labeling method could result in final labeling with more than one fluorophore per monomer, one binds to the N-terminal domain and the second to the single lysine of the polypeptide chain.

In this work, we aim to elucidate whether these unwanted effects can be avoided by using tailored labeling. For this purpose, we investigated the *in vitro* aggregation of α-syn, which is significantly larger (MW ~14 kDa) than the peptides described above. Furthermore, a site-specific labeling method was used to covalently label the C-terminal group of the peptide, an area of the polypeptide chain scarcely involved in fibrillation as confirmed by recent cryo-electron microscopy structures.[15,20,22] In this way, a single fluorophore per monomer was present and in a defined position along the protein polypeptide chain. Following a previously proposed labeling strategy,[15,23] we used a variant of α-syn monomer, with a cysteine residue at the C-terminus of the peptide. We then used ATTO488 with a functional maleimide group that covalently binds to the cysteine at the C-terminal domain.

Correlative AFM–STED technique has been applied on site-specific labeled α-syn fibrils. By qualitative analysis, we observed that all, or at least the great majority, of the fibrillar aggregates displayed by AFM, were also visible in the STED image (Fig. 2), verifying that the fluorescent dye labels do not interfere with the aggregation process in a site-specific labeling method.

Nevertheless, the mean co-localization ratio between AFM and STED obtained from all the acquired images was quantified, following the methods described in Experimental, as 0.76 ± 0.22 (mean ± SD), calculated from 43 images derived from 15 different samples. However, in some of the images, we noted a lack of overlap in large portions of the images (Fig. S4†). This effect was mainly due to the optical distortions that precluded perfect correlation,[11] generating outliers that invalidate the results obtained from a restricted group of images. Repeating the analysis, excluding the images showing clear misalignment, we obtained a co-localization ratio of 0.87 ± 0.10, (calculated from 33 images). We also applied Chauvenet's criterion for the rejection of the outliers, a consolidated statistical method, obtaining a co-localization ratio of 0.84 ± 0.12. Fig. 4 shows the statistical distribution of the data

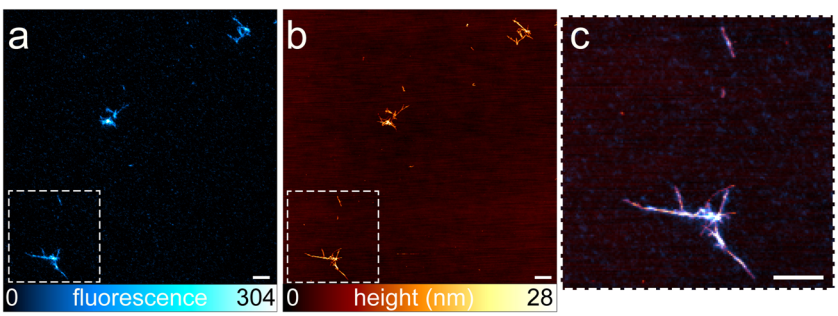

Fig. 2 Representative fibrils containing α-syn site-specific labeled with ATTO488-maleimide at a dye-to-protein ratio of 1 : 22 visualized by STED microscopy (a), AFM (b), and the correlative AFM–STED microscopy in a zoomed area of the image (c). All the population of fluorescent fibrils visualized by AFM is also visible in the STED image (a and b), confirming that the presence of fluorescent dye does not interfere with the aggregation process. Fibrils appear entirely and homogeneously labeled (c). The ratio of co-localization calculate for image c is 0.97 (f). Scale bars: 1 μm (a–c). Other images of fibrils from site-specific labeled α-syn are shown in Fig. S5.†

after Chauvenet's criterion application. Our observations indicated that the great majority of the fibrillar aggregates were fluorescent.

As a comparative approach, we repeated the analysis labeling α-syn monomers with ATTO488-NHS, as previously done on insulin. We labeled α-syn monomers with 1.5 molar equivalent of the fluorophore, to have a low final concentration of fluorophore per peptide molecule. HPLC confirmed a high efficiency in the conjugation (higher than 90%, Fig. S1 in ESI†).

Fig. 3 shows fibrils obtained from α-syn labeled with ATTO488-NHS. A large population of unlabeled fibrils is present and displayed in the AFM image (Fig. 3b), confirming the coexistence of different aggregation pathways in which labeled molecules may engage, in agreement with what has been previously observed in experiments performed on insulin fibrils.[12] The co-localization ratio calculated on 8 images from 4 different samples was 0.30 ± 0.16. Applying Chauvenet's criterion, we excluded one outlier obtaining a final co-localization ratio of 0.26 ± 0.08 (see also Fig. 4). Although, AFM analysis demonstrated that fibrils labeled with ATTO488-NHS were significantly thinner, we did not reveal a direct correlation between the fibril thickness and the presence of fluorescence. Although the preparation procedure of α-syn suggested the absence of any fibrillar aggregate before the aggregation process started, to further exclude the possibility to have unlabeled fibrils already present in the initial solution we performed AFM imaging on both the unlabeled α-syn and α-syn just after the labeling with ATTO488-NHS. The results are shown in Fig. S6.†

In this approach, we lost the precise control over the position of the fluorophore along the polypeptide chain, because 15 lysines (Lys) are present in the α-syn sequence. The number of Lys residues in α-syn is high, compared to the case of insulin. In particular, 11 Lys are located in the N-terminal domain (1–60), 1 in the central NAC region (61–95), and 3 at the C-terminus (96–140) (Fig. 5).[24] We note that 2 of the 3 Lys of C-terminus are the first two amino acids of this domain, close to the NAC region. During the marking procedure, the dye molecules are randomly distributed, but they will have a high probability of binding the N-terminal domain. While the C-terminal domain is not strongly involved in aggregation, the N-terminal plays a fundamental, although not fully understood, role. In particular, a short motif in the N-terminal region is crucial for aggregation. Doherty *et al.*[25] demonstrated that the 7-residue sequence, 36–42, controls α-syn aggregation. Deletion of this sequence prevents aggregation at pH 7.5 *in vitro*. The 36–42 sequence (GVLYVGS) contains no lysines, but lysines surround this short motif: sequence 30–45 is fact GKTKEGVLYVGSKTK, in which four lysines appear. The presence of fluorophores in this region probably results in significant, if not complete, suppression of protein aggregation capability. This could explain the lower total fluorescence emitted by fibrillar aggregates in samples with the ATTO488-NHS dye. The presence of a significant fluorescence background is an indirect proof of the presence of a non-fibrillar fraction with a high content of labeled peptides. Small fluorescent aggregates are displayed in Fig. 3c. These features are not correlated to AFM topography; a detailed discussion on this issue is

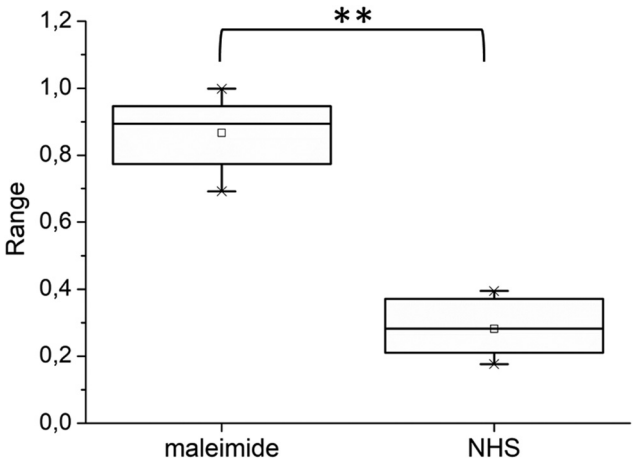

Fig. 4 The co-localization ratio obtained for fibrils obtained in the presence of protein monomers labeled using ATTO 488-maleimide (left) and ATTO 488-NHS (right) functional groups are significantly different (**$P < 0.01$).

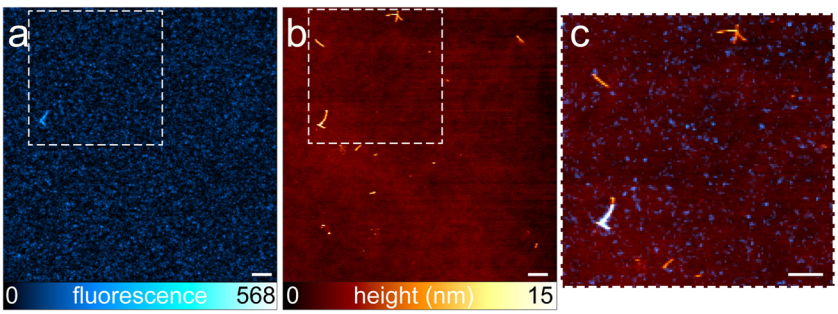

Fig. 3 Representative fibrils containing α-syn labeled with ATTO488-NHS at a dye-to-protein ratio of 1 : 22. STED image (a), AFM image (b), and the correlative AFM–STED image obtained in the area of the inset (c). A large population of fibrils is not fluorescent, and is not displayed in the STED image. Only one of the larger fibrils is displayed with both imaging modalities. The ratio of co-localization is 0.26. The scale bar is 1 μm (a–c). Other images of fibrils from ATTO488-NHS labeled α-syn are shown in Fig. S7.†

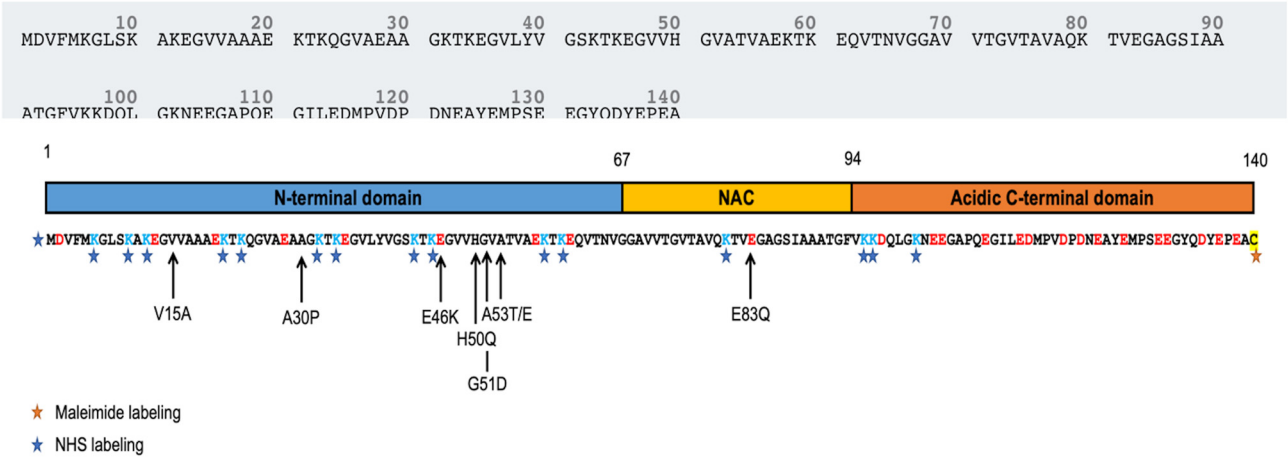

Fig. 5 Scheme indicating the position of published pathological mutations of α-syn inducing parkinsonism and the comparison of possible labeling site using maleimide chemistry to C-terminal cysteine (orange star) or NHS chemistry to primary amines (blue stars).

reported in Fig. S8.† Furthermore, N-terminus lysine residues contribute to the formation of a hydrophilic tunnel that plays a stabilizing effect in the interfacial region of two protofilaments.[22] Of note, most of the point mutations associated to pathological progression are located at the N-terminal domain, mainly close to the NAC region (Fig. 5).[26–30] All these findings, supported the idea of a key role played by N-terminal region in α-syn aggregation. The contribution to fibril formation of an α-syn monomer functionalized with a hydrophobic fluorophore in the N-terminal domain is probably not favored for steric and hydrophobicity reasons. In a scenario characterized by a high level of polymorphism,[31] the labeled monomers participate as building blocks in a limited subpopulation of fibrils, although the resolution of the AFM was not sufficient to detect any structural difference between fluorescent and non-fluorescent aggregates. In these samples, we observed that a large number of fibrils were not fluorescent, and the coexistence of labeled and unlabeled aggregates was evident.

Conclusions

In this investigation, focusing on *in vitro* aggregation of α-syn, we demonstrated that the position of covalently bound fluorophores along the polypeptide chain is crucial in determining the role that the labeled peptides might play in the fibrillation process. In particular, the large molecular size alone is not sufficient to avoid influence on the peptide aggregation upon binding with a fluorescent dye molecule. This work suggests the application of a site-specific labeling method, targeting the portion of the protein not involved in aggregation, *i.e.*, the C-terminus in the case of α-syn. The design of specific fluorophore conjugation strategies is advisable for the study of any intermolecular process. AFM–STED correlative microscopy is therefore a candidate as a gold standard method for monitoring fluorophore influence in several molecular processes and stands out from the bulk methods applied in aggregation kinetics analysis as it allows the investigation of individual fibrillar products.

Author contributions

S. J. and C. C. performed AFM imaging, S. J. and P. B. performed STED imaging; C. C., S. D., and A. D. conceptualized the work; L. C., L. T., M. S. and L. B. prepared fluorescently labelled α-syn, amyloid fibrils, and performed TEM imaging and HPLC; all the authors wrote and revised the manuscript.

Conflicts of interest

There is no conflict to declare.

Acknowledgements

This work has been performed under the project DIFILAB of the Università degli Studi di Genova. The work has been supported by the Università degli Studi di Genova and Italian Ministry of Education (grant RBAP11ETKA-005), and by the Molecular Scale Biophysics Research Infrastructure (MOSBRI, grant agreement number: 101004806—H2020-INFRAIA-2018-2020/H2020-INFRAIA-2020-1).

References

1 I. J. Hardy and W. G. Cook, Predictive and correlative techniques for the design, optimisation and manufacture of solid dosage forms, *J. Pharm. Pharmacol.*, 2010, **55**, 3–18, DOI: **10.1111/j.2042-7158.2003.tb02428.x**.
2 T. Ando, S. P. Bhamidimarri, N. Brending, H. Colin-York, L. Collinson, N. De Jonge, P. J. de Pablo, E. Debroye,

C. Eggeling, C. Franck, M. Fritzsche, H. Gerritsen, B. N. G. Giepmans, K. Grunewald, J. Hofkens, J. P. Hoogenboom, K. P. F. Janssen, R. Kaufmann, J. Klumperman, N. Kurniawan, J. Kusch, N. Liv, V. Parekh, D. B. Peckys, F. Rehfeldt, D. C. Reutens, M. B. J. Roeffaers, T. Salditt, I. A. T. Schaap, U. S. Schwarz, P. Verkade, M. W. Vogel, R. Wagner, M. Winterhalter, H. Yuan and G. Zifarelli, The 2018 correlative microscopy techniques roadmap, *J. Phys. D: Appl. Phys.*, 2018, **51**, 443001, DOI: 10.1088/1361-6463/aad055.

3 S. Jadavi, P. Bianchini, O. Cavalleri, S. Dante, C. Canale and A. Diaspro, Correlative nanoscopy: A multimodal approach to molecular resolution, *Microsc. Res. Tech.*, 2021, **84**, 2472–2482, DOI: 10.1002/jemt.23800.

4 A. V. Agronskaia, J. A. Valentijn, L. F. van Driel, C. T. W. M. Schneijdenberg, B. M. Humbel, P. M. P. van Bergen en Henegouwen, A. J. Verkleij, A. J. Koster and H. C. Gerritsen, Integrated fluorescence and transmission electron microscopy, *J. Struct. Biol.*, 2008, **164**, 183–189, DOI: 10.1016/j.jsb.2008.07.003.

5 B. Knierim, B. Luef, P. Wilmes, R. I. Webb, M. Auer, L. R. Comolli and J. F. Banfield, Correlative microscopy for phylogenetic and ultrastructural characterization of microbial communities: Correlative TEM and CARD-FISH imaging, *Environ. Microbiol. Rep.*, 2012, **4**, 36–41, DOI: 10.1111/j.1758-2229.2011.00275.x.

6 S. Redemann and T. Müller-Reichert, Correlative light and electron microscopy for the analysis of cell division: CLEM FOR ANALYSIS OF CELL DIVISION, *J. Microsc.*, 2013, **251**, 109–112, DOI: 10.1111/jmi.12056.

7 F. J. Timmermans and C. Otto, Contributed Review: Review of integrated correlative light and electron microscopy, *Rev. Sci. Instrum.*, 2015, **86**, 011501, DOI: 10.1063/1.4905434.

8 B. Harke, J. V. Chacko, H. Haschke, C. Canale and A. Diaspro, A novel nanoscopic tool by combining AFM with STED microscopy, *Opt. Nanosc.*, 2012, **1**, 3, DOI: 10.1186/2192-2853-1-3.

9 J. V. Chacko, B. Harke, C. Canale and A. Diaspro, Cellular level nanomanipulation using atomic force microscope aided with superresolution imaging, *J. Biomed. Opt.*, 2014, **19**, 1, DOI: 10.1117/1.JBO.19.10.105003.

10 J. V. Chacko, F. C. Zanacchi and A. Diaspro, Probing cytoskeletal structures by coupling optical superresolution and AFM techniques for a correlative approach, *Cytoskeleton*, 2013, **70**, 729–740, DOI: 10.1002/cm.21139.

11 J. V. Chacko, C. Canale, B. Harke and A. Diaspro, Sub-Diffraction Nano Manipulation Using STED AFM, *PLoS One*, 2013, **8**, e66608, DOI: 10.1371/journal.pone.0066608.

12 M. Cosentino, C. Canale, P. Bianchini and A. Diaspro, AFM-STED correlative nanoscopy reveals a dark side in fluorescence microscopy imaging, *Sci. Adv.*, 2019, **5**, eaav8062, DOI: 10.1126/sciadv.aav8062.

13 C. Xue, T. Y. Lin, D. Chang and Z. Guo, Thioflavin T as an amyloid dye: fibril quantification, optimal concentration and effect on aggregation, *R. Soc. Open Sci.*, 2017, **4**, 160696, DOI: 10.1098/rsos.160696.

14 S. Sharma, P. Modi, G. Sharma and S. Deep, Kinetics theories to understand the mechanism of aggregation of a protein and to design strategies for its inhibition, *Biophys. Chem.*, 2021, **278**, 106665, DOI: 10.1016/j.bpc.2021.106665.

15 D. Pinotsi, A. K. Buell, C. Galvagnion, C. M. Dobson, G. S. Kaminski Schierle and C. F. Kaminski, Direct Observation of Heterogeneous Amyloid Fibril Growth Kinetics via Two-Color Super-Resolution Microscopy, *Nano Lett.*, 2014, **14**, 339–345, DOI: 10.1021/nl4041093.

16 P. Mahou, N. Curry, D. Pinotsi and G. K. Schierle, Simulated Emission Depletion microscopy to study amyloid fibril formation, *Proc. SPIE*, 2015, **10**, 9331, DOI: https://doi.org/10.1117/12.2079320.

17 W. Hoyer, D. Cherny, V. Subramaniam and T. M. Jovin, Impact of the Acidic C-Terminal Region Comprising Amino Acids 109–140 on α-Synuclein Aggregation in Vitro, *Biochemistry*, 2004, **43**, 16233–16242, DOI: 10.1021/bi048453u.

18 M. Vilar, H.-T. Chou, H. Stahlberg and R. Riek, The fold of α-synuclein fibrils, *Proc. Natl. Acad. Sci. U. S. A.*, 2008, **105**(25), 8637–8642, DOI: 10.1073/pnas.0712179105.

19 L. Streubel-Gallasch, V. Giusti, M. Sandre, I. Tessari, N. Plotegher, E. Giusto, A. Masato, L. Iovino, I. Battisti, G. Arrigoni, D. Shimshek, E. Greggio, M.-E. Tremblay, L. Bubacco, A. Erlandsson and L. Civiero, Parkinson's Disease–Associated LRRK2 Interferes with Astrocyte-Mediated Alpha-Synuclein Clearance, *Mol. Neurobiol.*, 2021, **58**, 3119–3140, DOI: 10.1007/s12035-021-02327-8.

20 Y. Kim, S. O. Ho, N. R. Gassman, Y. Korlann, E. V. Landorf, F. R. Collart and S. Weiss, Efficient Site-Specific Labeling of Proteins via Cysteines, *Bioconjugate Chem.*, 2008, **19**, 786–791, DOI: 10.1021/bc7002499.

21 S. V. Costes, D. Daelemans, E. H. Cho, Z. Dobbin, G. Pavlakis and S. Lockett, Automatic and Quantitative Measurement of Protein-Protein Colocalization in Live Cells, *Biophys. J.*, 2004, **86**, 3993–4003, DOI: 10.1529/biophysj.103.038422.

22 R. Guerrero-Ferreira, N. M. Taylor, D. Mona, P. Ringler, M. E. Lauer, R. Riek, M. Britschgi and H. Stahlberg, Cryo-EM structure of alpha-synuclein fibrils, *eLife*, 2018, **7**, e36402, DOI: 10.7554/eLife.36402.

23 M. Pivato, G. De Franceschi, L. Tosatto, E. Frare, D. Kumar, D. Aioanei, M. Brucale, I. Tessari, M. Bisaglia, B. Samori, P. P. de Laureto and L. Bubacco, Covalent α-Synuclein Dimers: Chemico-Physical and Aggregation Properties, *PLoS One*, 2012, **7**, e50027, DOI: 10.1371/journal.pone.0050027.

24 F. Emamzadeh, Alpha-synuclein structure, functions, and interactions, *J. Res. Med. Sci.*, 2016, **21**, 29, DOI: 10.4103/1735-1995.181989.

25 C. P. A. Doherty, S. M. Ulamec, R. Maya-Martinez, S. C. Good, J. Makepeace, G. N. Khan, P. van Oosten-Hawle, S. E. Radford and D. J. Brockwell, A short motif in the N-terminal region of α-synuclein is critical for both aggregation and function, *Nat. Struct. Mol. Biol.*, 2020, **27**, 249–259, DOI: 10.1038/s41594-020-0384-x.

26 A. P. Kiely, Y. T. Asi, E. Kara, P. Limousin, H. Ling, P. Lewis, C. Proukakis, N. Quinn, A. J. Lees, J. Hardy, T. Revesz, H. Houlden and J. L. Holton, α-Synucleinopathy associated with G51D SNCA mutation: a link between Parkinson's disease and multiple system atrophy?, *Acta Neuropathol.*, 2013, **125**, 753–769, DOI: **10.1007/s00401-013-1096-7**.

27 C. Proukakis, C. G. Dudzik, T. Brier, D. S. MacKay, J. M. Cooper, G. L. Millhauser, H. Houlden and A. H. Schapira, A novel α-synuclein missense mutation in parkinson disease, Clinical/Scientific Notes, *Am. Acad. Neurol.*, 2013, **80**, 3.

28 P. Pasanen, L. Myllykangas, M. Siitonen, A. Raunio, S. Kaakkola, J. Lyytinen, P. J. Tienari, M. Pöyhönen and A. Paetau, A novel α-synuclein mutation A53E associated with atypical multiple system atrophy and Parkinson's disease-type pathology, *Neurobiol. Aging*, 2014, **35**, 2180.e1–2180.e5, DOI: **10.1016/j.neurobiolaging.2014.03.024**.

29 A. Kapasi, J. R. Brosch, K. N. Nudelman, S. Agrawal, T. M. Foroud and J. A. Schneider, A novel *SNCA*, E83Q mutation in a case of dementia with Lewy bodies and atypical frontotemporal lobar degeneration, *Neuropathology*, 2020, **40**, 620–626, DOI: **10.1111/neup.12687**.

30 K. Daida, S. Shimonaka, K. Shiba-Fukushima, J. Ogata, H. Yoshino, A. Okuzumi, T. Hatano, Y. Motoi, T. Hirunagi, M. Katsuno, H. Shindou, M. Funayama, K. Nishioka, N. Hattori and Y. Imai, α-Synuclein V15A Variant in Familial Parkinson's Disease Exhibits a Weaker Lipid–Binding Property, *Mov. Disord.*, 2022, **37**(10), 2075–2085, DOI: **10.1002/mds.29162**.

31 M. Landureau, V. Redeker, T. Bellande, S. Eyquem and R. Melki, The differential solvent exposure of N-terminal residues provides "fingerprints" of alpha-synuclein fibrillar polymorphs, *J. Biol. Chem.*, 2021, **296**, 100737, DOI: **10.1016/j.jbc.2021.100737**.